Chapter 8

Interdigitated MEMS Supercapacitor for Powering Heart Pacemaker

Hafzaliza Erny Zainal Abidin, Azrul Azlan Hamzah, Jumril Yunas, Mohd Ambri Mohamed and Burhanuddin Yeop Majlis

Additional information is available at the end of the chapter

http://dx.doi.org/10.5772/65127

Abstract

Power MEMS can be defined as microelectromechanical systems for power generation and energy conversion. Energy harvesting has become an increasingly popular option for powering electronic devices as a long-lasting power source. Energy scavenging is defined as the process by which the energy is derived such as vibration, solar, wind, and thermal. Energy harvesting from the environment can prolong the life cycle and reduce the maintenance costs of electronic devices. Among the various sources of energy storage, Among the various of energy storage, supercapacitor has recently gained much interest in fields such as bioMEMS, biomedical implants and power electronic devices due to its advantages such as high power density, rapid charge and discharge and unlimited number of recharge cycles. In biomedical and bioMEMS systems, an energy storage device is needed to power other active biomedical devices within the system. For implantable devices such as a heart pacemaker, the power requirement is in the range of 30–100 μW. Microsupercapacitors play an important role in energy harvesting system, such as collecting energy from ambient energy sources. Human body is very resourceful in generating micropower in the form of heat dissipation, deformation of elastic tissue, and motion. Due to the advantages of MEMS energy harvesting system, the system can be use widely for biomedical implant devices, such as heart pacemakers and hearing aids, and can be used for a long time and without the need for battery replacement. In this work, planar and double-stacked interdigital electrode supercapacitor designs were modeled using Coventorware software. From simulation, it is observed that for planar structure, the specific capacitance is 0.22 mF/cm^{-2}, and for double-stacked structure specific capacitance can be increased to 0.48 mF/cm^{-2}. In terms of specific power, the planar structure produces 0.99 mW/cm^{-2}, and the double-stacked structure produces 2.18 mW/cm^{-2}. These results highlight the superiority of the double-stacked MEMS interdigital supercapacitor design compared with its planar counterpart

in terms of charging capacity and electrical performance, thus making it favorable for powering heart pacemaker.

Keywords: energy scavenging, interdigital electrode microsupercapacitor, heart pacemaker, Coventorware

1. Introduction

Biomedical implantable devices usually required micro power sources with smaller dimensions and higher power density. The output power generated is in the range of nanowatt to microwatt. Power requirement for implantable devices for heart pacemaker is 30-100 μW [1, 2]. An energy generation system producing power within that range would qualify as a probable candidate to replace the conventional battery system. Typically, a Lithium-ion battery is widely used in biomedical implants such as pacemakers. However, batteries have many disadvantages such as short lifetime and contain a finite amount of depletable chemical energy [3]. Thus, patients using biomedical implants devices such as cardiac pacemakers have to replace the battery once every 5 years to 10 years. To avoid frequent battery replacement, a renewable energy generation and storage system could become a vital solution to infinitely empower biomedical devices, without the need for any powering unit replacement [4, 5].

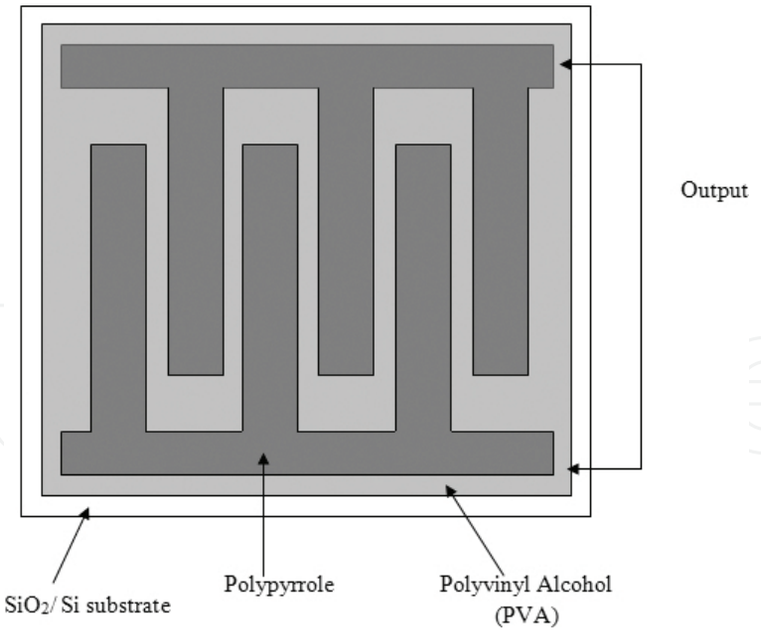

Figure 1. 2D view of planar interdigital electrode supercapacitor [23].

MEMS is one of the fundamental area that consists of mechanical, electrical, chemical, optical, and fluids engineering and integrated to the MEMS such as micropump,microvalve,microneedles and micronozzles [6–8]. Supercapacitor has high potential to replace conventional

http://dx.doi.org/10.5772/65127

battery usage due to its high power density, rapid charge and discharge, long cycle life, high energy densities and unlimited number of recharge cycles. Miniaturized electrochemical capacitor or micro supercapacitor has promising capability to power small electronic devices. [9–11]. Supercapacitors have the capability to store up to 10,000 times more energy compared with its conventional counterparts [12, 13]. For electrode structure design of a supercapacitor, it can be classified into interdigital, sandwich, and roll structure [14]. Interdigital electrodes structure has their advantages such as low charging current, reduced solution resistance effects, and diffusion controllable current [15].

Conducting polymers have high capacitance and high conductivity with low cost compared to carbon as the electrode material for supercapacitor [16, 17]. Conducting polymers such as Polypyrrole (PPY), Polyaniline (PANI), and Polythiophene are mostly used as the electrode material in supercapacitors due to its advantages such as easy fabrication, low cost, high charge density, good conductivity, and more flexible [18–21]. In terms of electrolyte, Polyvinyl Alcohol (PVA) has been chosen due to its high charging density and low cost [22].

Planar interdigital electrode supercapacitor with polypyrrole (Ppy) – polyvinyl alcohol (PVA) as electrodes coating and electrolyte material respectively was first introduced by Wei Sun and Xuyuan Chen, having the advantage of high charging capacity due to its interdigital structure. In this structure, the supercapacitor consists of two Ppy coated nickel electrodes as current collectors and PVA as a solid-state electrolyte (**Figure 1**) [23].

In addition, carbon nano tube (CNT) can also be used as electrodes for the supercapacitor. In 2009, Jiang et al. [24] used carbon nano tube as supercapacitor electrodes and produced a specific capacitance of 428 μF/cm^2 and a power density of 0.28 mW/cm^2. In 2011, Shen et al. have used an activated carbon as part of a supercapacitor material to obtain a larger surface area. Beidaghi and Wang 2011 [25] also used carbon as supercapacitor electrodes to increase the surface area to be more effective but had to be improved in terms of ion diffusion through the thickness of the dielectric film for the electrodes.

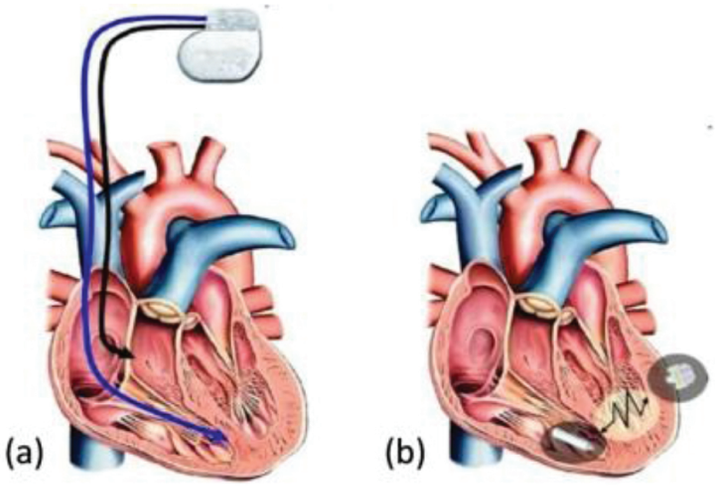

Figure 2. (a) Current pacemaker; (b) Future pacemaker using energy harvesting. Source: http://www.eetimes.com [26].

Microsupercapacitors play an important role in the energy harvesting system such ascollecting energy from ambient energy sources. In energy harvesting systems, it does not require any chemicals. In fact, the human body is very flexible in generating power from heat dissipation, deformation of elastic tissue, and the others. Due to its advantages as a energy harvesting system, it can be used widely for biomedical implant devices such as pacemakers and hearing aids and can be used for a long time and recharge without any replacement. **Figures 2** and **3** show examples of supercapacitor applications in MEMS devices. For a current pacemaker as depicted in **Figure 2**, the batteries are frequently changed and required a high cost for surgical operations compared with a pacemaker using energy harvesting that is more reliable and comfortable to the patients. For a normal pacemaker as shown in **Figure 2(a)**, it consists of two elements which are first, a pulse generator, placed under the skin in the chest, a battery, and the impulse control system, and second, a lead inserted directly in the heart through a vein, delivering the impulses [26]. **Figure 3** shows a small chip in the middle-ear cavity. The main components are the surgical implant, which is placed underneath the skin, and externally the audio processor that converts sound into electrical signals [26].

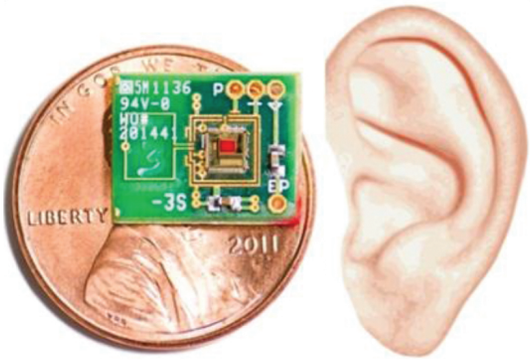

Figure 3. Small chip in the middle-ear cavity. Source: http://www.eetimes.com [26].

2. Design of planar interdigital electrode MEMS supercapacitor

In this research, planar interdigital electrode supercapacitor design was modeled using Coventorware ver.2008 via its process simulator tool. The software uses finite element analysis [27]. The planar supercapacitor structure consists of silicon (Si), silicon oxide (SiO_2), nickel (Ni), Polypyrrole (Ppy), and Polyvinyl Alcohol (PVA) layers. The structure was initiated by setting silicon as substrate 200 nm SiO_2 that was deposited on the silicon layer. Interdigital electrode structure was patterned using Ni on the SiO_2 layer. After that, the seed nickel layer was electroplated to construct high aspect ratio of nickel [28, 29]. The Ni electrodes were coated with Ppy to create the dielectric layer. PVA layer was fill deposited between the fingers to function as solid-state electrolyte. The process flow for modeling the structure of planar interdigital electrode supercapacitor is as shown in **Figure 4** and three-dimension structure of planar interdigital electrode supercapacitor is as shown in **Figure 5**.

http://dx.doi.org/10.5772/65127

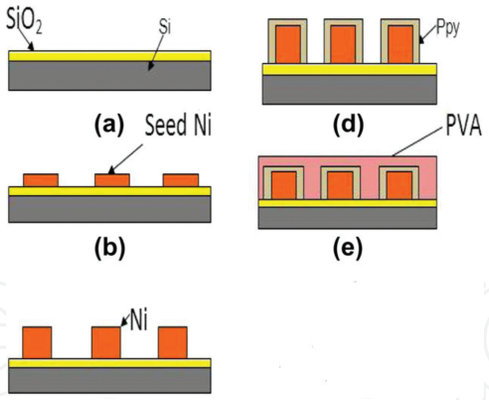

Figure 4. Process flow for modeling the double-stacked supercapacitor. (a) SiO_2 deposition, (b) Seed Ni deposition and patterning of 2D layout interdigital structure, (c) Ni growth of the interdigital structure, (d) Ppy coating on Ni, (e) PVA filling.

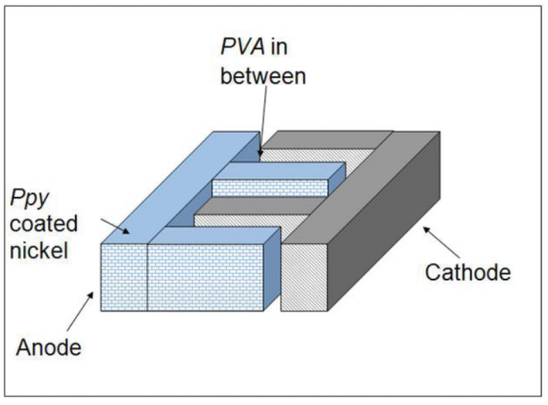

Figure 5. Structure of planar interdigital electrode supercapacitor.

3. Design of double-stacked interdigital electrode MEMS supercapacitor

Double-stacked supercapacitor design was modeled using Coventorware ver.2008 via its process simulator tool. The double-stacked supercapacitor structure consists of Si, SiO_2, Ni,

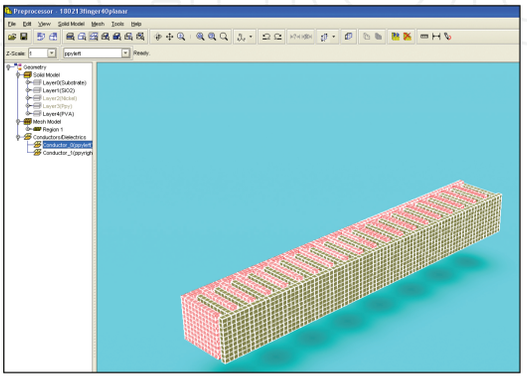

Figure 6. Meshing structure of planar interdigital electrode supercapacitor.

Ppy, and PVA layers. For a double-stacked structure, the mirrored cell from initial cell was developed by similar process steps. The electrodes would lie next to and atop of each other when the two cells are sandwiched together. The structure was initiated by setting silicon as substrate. 200 nm SiO2 was stack deposited on the silicon layer. Interdigital electrode structure was patterned using Ni on the SiO_2 layer. The Ni electrodes were coated with Ppy to create the dielectric layer. PVA layer was deposited between the fingers to function as a solid-state electrolyte (**Figures 6–9**).

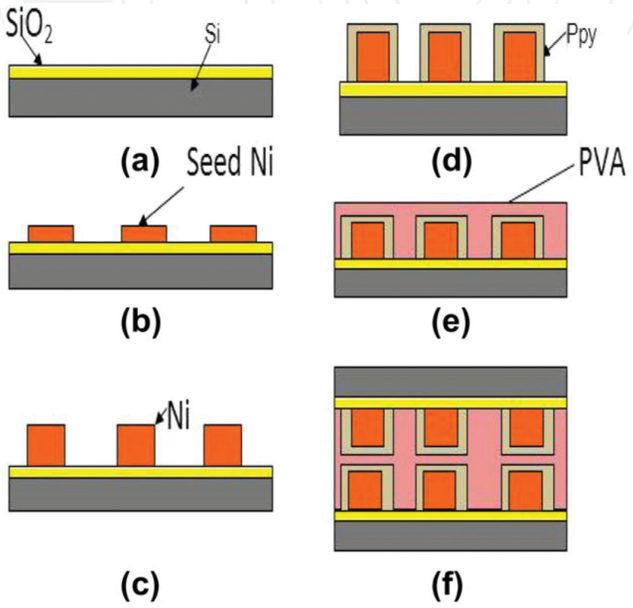

Figure 7. Process flow for modeling the double-stacked supercapacitor. (a) SiO2 deposition, (b) Seed Ni deposition and patterning of 2D layout interdigital structure, (c) Ni growth of the interdigital structure, (d) Ppy coating on Ni, (e) PVA filling and (f) Double-stack attachment.

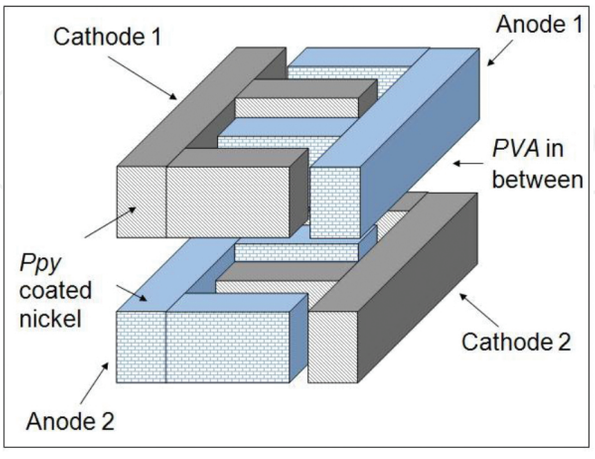

Figure 8. Structure of double-stacked interdigital supercapacitor with interwoven electrodes. Note that anode and cathode are always next to each other in bottom–bottom, top–top, and top–bottom electrode pairing configurations for the double-stacked design.

http://dx.doi.org/10.5772/65127

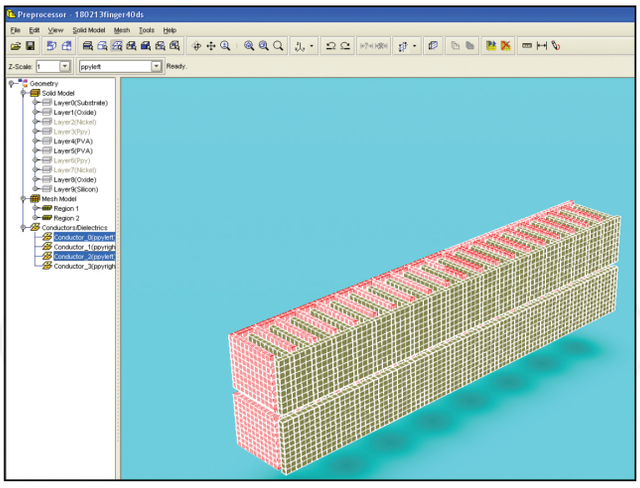

Figure 9. Meshing structure double-stacked interdigital electrode supercapacitor.

4. Electrical characteristics for planar interdigital electrode supercapacitor

Comsol Multiphysics ver.4.2 simulation tool was used to simulate the electrical characteristic of planar interdigital electrode design. Secondary current distribution and transport of diluted are chosen as the application modules [30]. Two dimensional time dependent cyclic voltammetry model was developed for the interdigital structure. Cyclic voltammetry measures current response when potential is applied to the working electrodes. For interdigital structure, the boundary conditions define the interface between the electrode and the electrolyte. The applied voltage range is set to −0.5 V to 0.5 V at the working electrode, and the current response at the working electrode can be measured. In the structure, Ppy-coated nickel is the current collector and PVA is the solid-state electrolyte. For the interdigital electrode, it consists of two electrode which is working electrode and counter electrode. The boundary conditions can be identify the interface between electrode and electrolyte. We set the boundaries at the counter electrode as ground and the electrode potential was applied at the working electrode boundaries based on 1[V]/Scan (t/1[s])-0.5[V] function [31, 32].

For cyclic voltammetry simulation, the bidirectional reaction can be formulated as in Ref. [3]:

$$A + e \underset{\leftarrow}{\overset{\rightarrow}{}} B \tag{1}$$

According to Eq. (2), for mass flow density of forward reaction N_f, it can be expressed as the rate constant k_f multiplied by concentration species during oxidation process C_O. For backward reaction, according to Eq. (3), for mass flow density of backward reaction N_b, it can be expressed as the rate constant k_b multiplied by concentration species during reduction process C_R.

$$N_f = k_f.Co \tag{2}$$

$$N_b = k_b.C_R \tag{3}$$

The rate constants of forward and backward reaction at the electrodes are described by the Butler-Volmer reaction kinetics

$$k_f = k_s e - \alpha\left(E - E_0\right)\frac{F}{RT} \tag{4}$$

$$k_b = k_s e\left(1-\alpha\right)\left(E - E_0\right)\frac{F}{RT} \tag{5}$$

where k_s is the standard rate constant and α is the transfer coefficient. In symmetrical reactions, α has a value 0.5. E is the applied voltage on the electrode interface and E_0 has a value 0 V. For F, R, and T, it is a Faraday constant (96485 C/mol), molar gas constant (8.3144 J mol^{-1} K^{-1}), and temperature (298 K), respectively.

Additionally, the relationship for current, potential, and concentration can be summarized as follows:

$$\frac{i}{nFA} = k0\{c_0 e[-\alpha\theta] - c_R e[(1-\alpha)\theta]\} \tag{6}$$

where $\theta = nF(E - E0)/RT$.

Initially, the Comsol simulation is simplified and performed on planar interdigital electrode structure as depicted in **Figure 8(a)**. It is observed that surface charge density is evenly distributed throughout the interdigital structures. As applied voltage between anode and cathode is slowly increased from 0 to 3 V, the charge density increases as more and more ions accumulate between the electrodes. A closer observation into the structure reveals that maximum charge density often occurs at the intersection of electrodes and its anchor, as depicted in **Figure 8(b)**. This is due to the proximity of the intersection point with the adjacent electrode, causing the charge to concentrate at the sharp edged points. The maximum charge density is as shown in **Figure 10(b)**.

Cyclic voltammetry portrays current response when potential is applied to the electrodes. In our case, the potential is applied at working electrode is between -0.5 V and 0.5 V, with the other electrode set as ground. The increasing voltage increases oxidation and reduction processes between the electrodes, driving current flow between working and counter electrodes. **Figure 11** shows that the oxidation and reductions occur within a voltage range of −0.5 and 0.5 V. For our design, ion flux reaches a peak within that region, resulting in maximum peak current (ip) of 6.0 A/m.

http://dx.doi.org/10.5772/65127

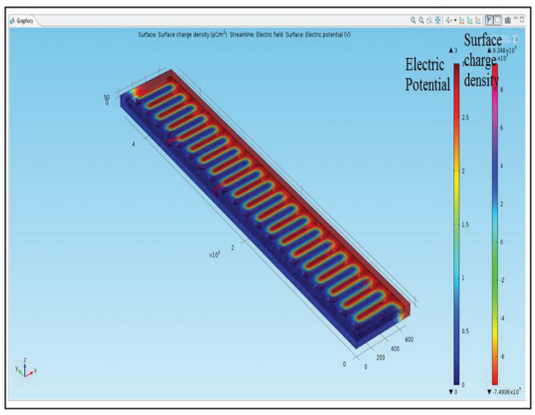

(a)

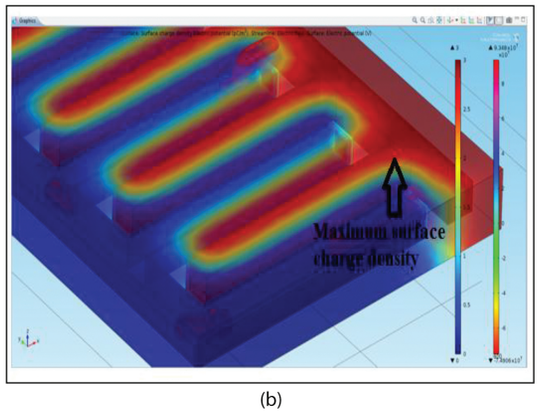

(b)

Figure 10. (a) Structure surface charge density; (b) Maximum surface charge density distributions of a planar supercapacitor with 20 finger pairs at an applied voltage of 3 V.

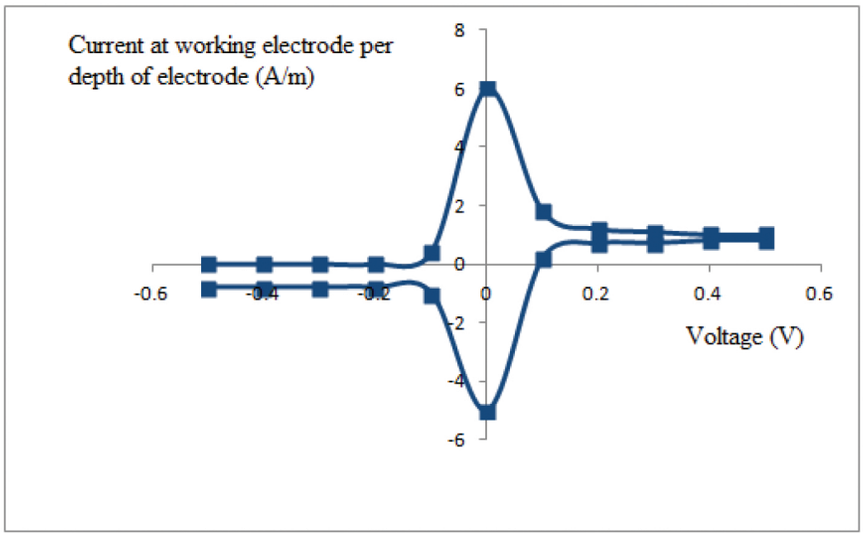

Figure 11. Cyclic voltammetry for planar interdigital electrode supercapacitor.

For a charge discharge of a microsupercapacitor, there are two techniques. One is the charging and discharging at a constant voltage to record current response with time, and the other is the charging discharging at a constant current to record the voltage response with time. In **Figure 12**, it is shown that when time is zero, the value of voltage is also zero. Discharging process for planar interdigital electrode occurred when the value of voltage decreased and was back to zero at 1 s.

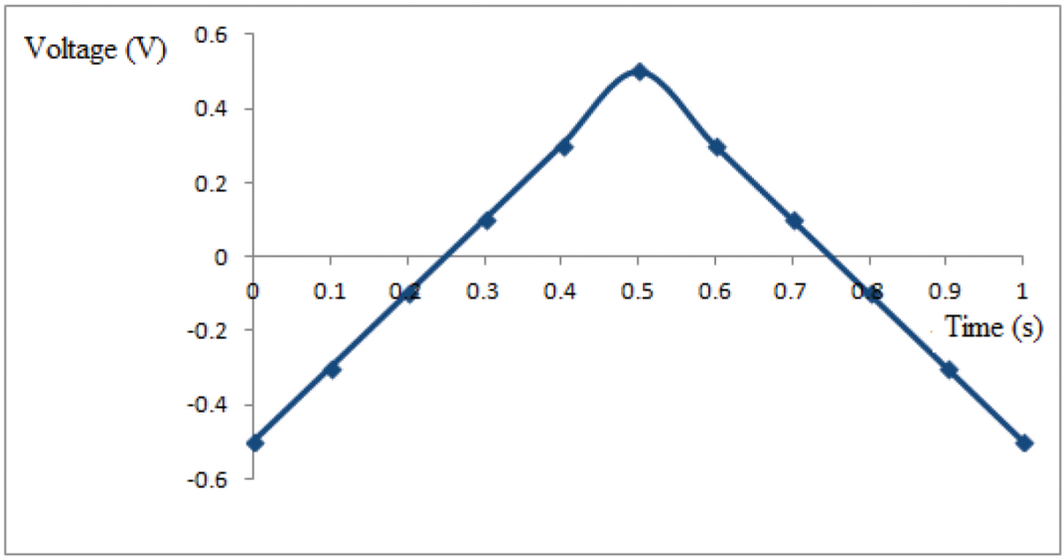

Figure 12. Charge discharge curve of planar electrode supercapacitor.

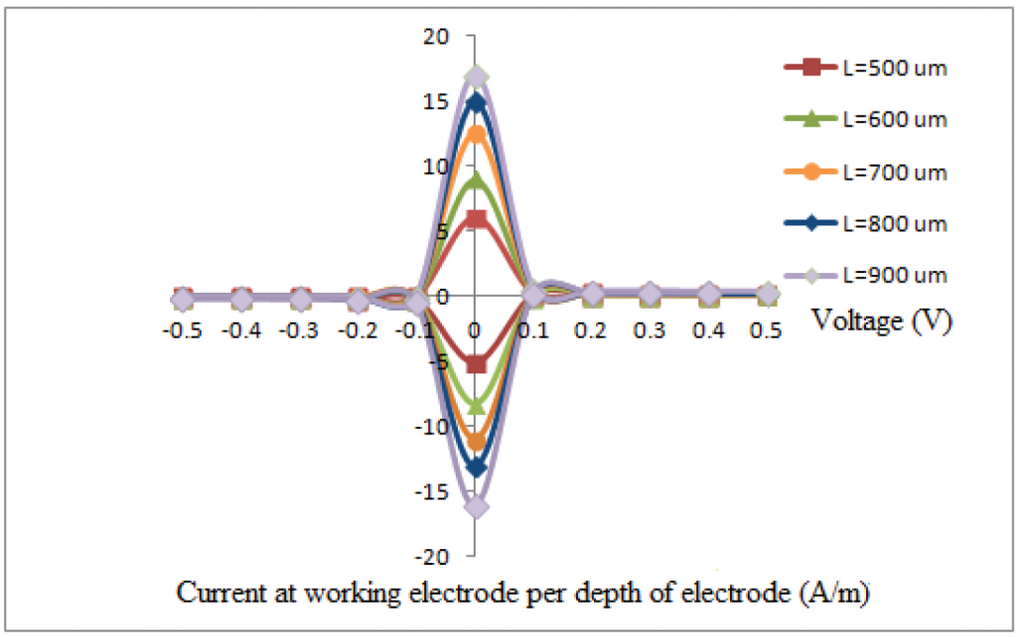

Figure 13. Cyclic voltammetry for various values of the length interdigital electrode.

http://dx.doi.org/10.5772/65127

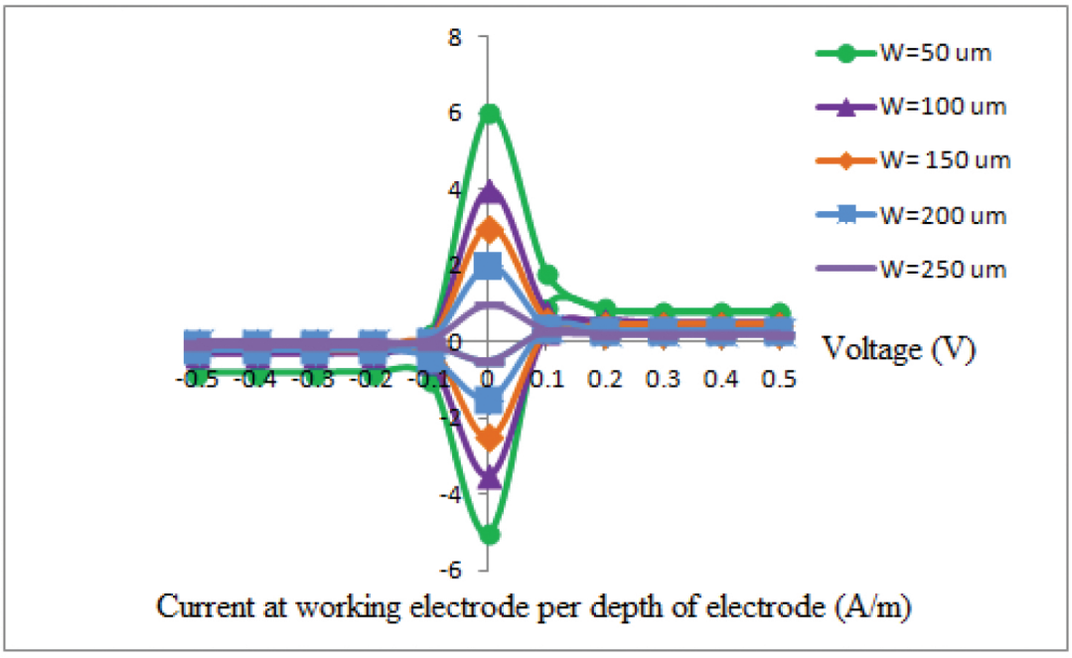

Figure 14. Cyclic voltammetry for various values of the width interdigital electrode.

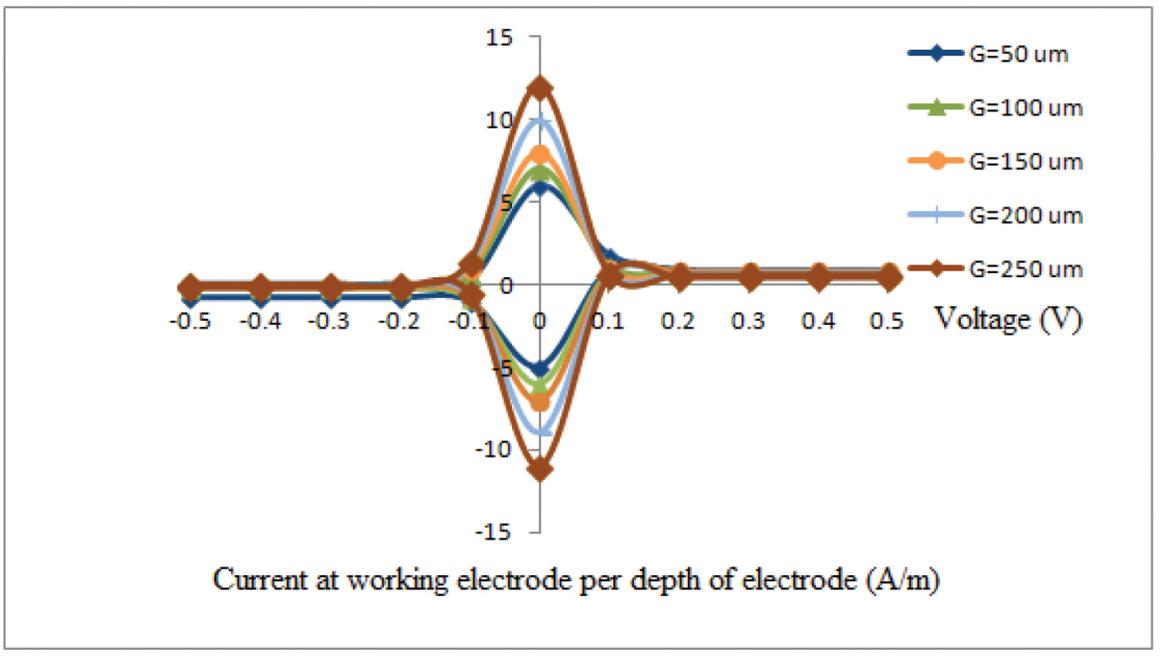

Figure 15. Cyclic voltammetry for various values of the gap interdigital electrode.

For the purposes of studying effects of design parameter changes, Comsol simulations were performed on the planar design with varying electrode length, width, and gap between the electrodes. Length of the interdigital electrodes are varied between 500 μm and 700 μm, with 700 μm being the maximum allowable length due to design limitation. From **Figure 13**, we can

see the longer the electrode, the higher the current response. The maximum current response achieved is 1.6 A/m corresponding to electrode length of 700 μm. Increasing electrode length increases active surface area, which in turn enable a higher redox activity between the electrodes. Thus, increasing electrode length increases current generating mass transport activity on the cyclic voltammetry. Adversely, increasing electrode width from 50 μm to 250 μm produces the opposite effect as shown in **Figure 14**. From the figure, we can see that the smaller the width, the higher the current response. The maximum value of current response is 0.9 A/m, which occurs at electrode width of 50 μm. The reactions occurs at working electrode per depth of electrode data because the modelling is done in 2-D. The increasing value of gap increases space between the electrodes. This allows higher amount of active species to be present at the active interface. At the working electrode, the reduction and oxidation occurs more and more rapidly as more electrolyte are available with the increasing gap (**Figure 15**).

5. Electrical characteristics for double-stacked interdigital electrode supercapacitor

Cyclic voltammetry for the determination of a plane design double-digit supercapacitor between MEMS is the same as determining the design for cycle voltammetry for a coplanar. But there is a slight difference compared with the maximum current value for the design of the plane. **Figure 16** shows that the maximum flow for the cycle voltammetry multiple planar design is 13.2 A/m, which is more than twice the maximum current value relative to the plane designs. In the process of oxidation and reduction, equilibrium is reached and is limited by the voltage on the electrode surface. In the redox cycle, a decrease in current flow is from the effects of depletion. To complete the cycle, the voltage is not only directed to the front but also, on the other hand, within the range specified above. The curved shape also depends on the scan rate. Scan rate can be described as the speed at which the potential is varied. In addition,

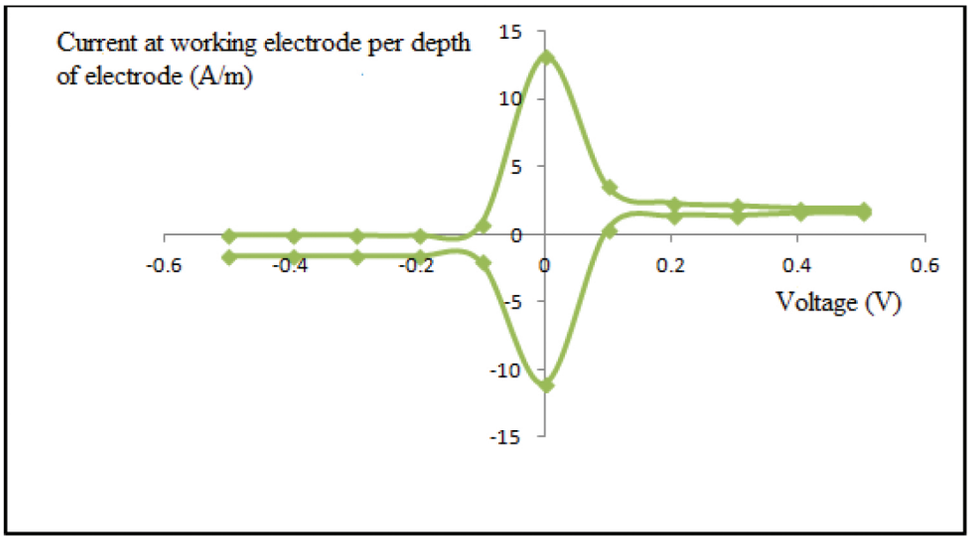

Figure 16. Cyclic voltammetry for double-stacked interdigital electrode supercapacitor.

http://dx.doi.org/10.5772/65127

Figure 17 shows the voltage response to the time indicated at 0.5 s, and the voltage reaches 1 V.

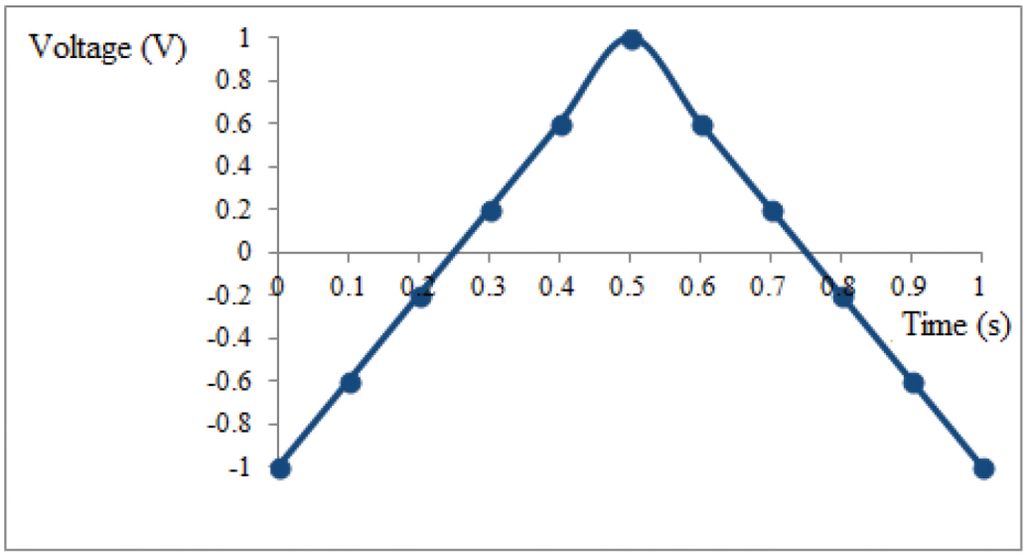

Figure 17. Charge discharge curve of double-stacked electrode supercapacitor.

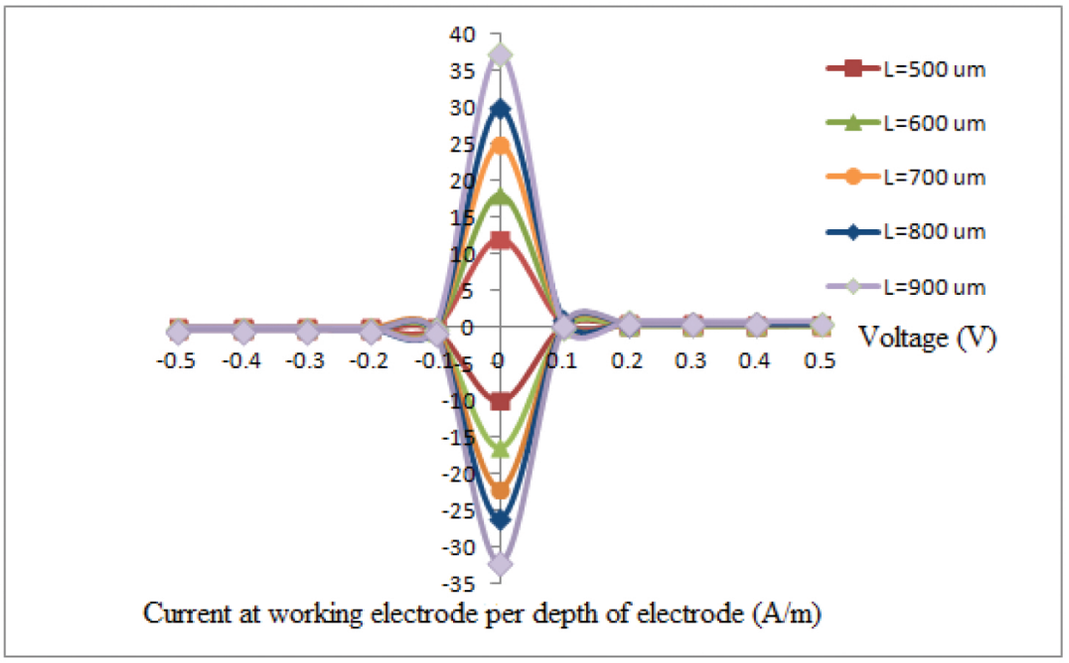

Figure 18. Cyclic voltammetry for various values of the length interdigital electrode.

Voltage is still in negative values until at t = 0.25 s. After that, the voltage increases until it reaches a maximum of 1.0 V at a value that is twice the value of the design of the plane at the time, t = 0.5 s, where the charging process occurs so as to achieve the maximum voltage. After

reaching the maximum voltage, the discharge process occurs, whereby the voltage drop causes the charging rate to reduce back to a negative value of −1.0 V at a time t = 1 s.

For the purpose of studying the effects of changes in response to the current design of the multiple-plane and the plane, the value for the electrode length, width, and the gap between the electrodes was varied as the design of the plane. The length of the electrode between the digits are 500 and 900 m, where the length of the electrode between the digit at 900 m is the maximum length allowed for the design limits. According to **Figure 18**, it can be seen that the more the length of the electrode, the higher the reaction flow. The maximum current response was obtained at 37.4 A/m to 900 m-long electrode. Increasing the length of the electrode leads to an increase in active surface area, which in turn allows a higher redox activity to occur between the electrodes. Therefore, increasing the length of the electrodes improves the mass transport activity generated during the cycle voltammetry. High flow shows the life cycle of a higher supercapacitor.

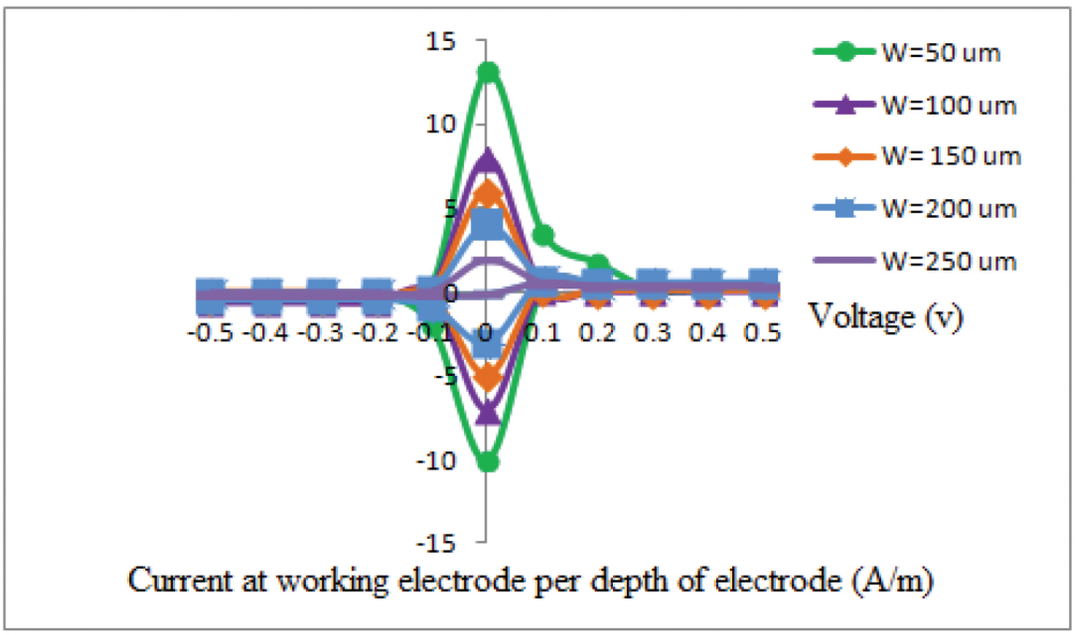

Figure 19. Cyclic voltammetry for various values of the width interdigital electrode.

According to **Figure 19**, we can see that the smaller the width of the electrode, the higher is the current response. The situation is similar to the design of the plane, and there is a difference in the maximum response current that is 13.2 A/m compared with 6.0 A/m for the design of the plane, which took place on the electrode width of 50 m. This phenomenon occurs because there is a balance between the surface area of the electrodes and the electrolyte. When the electrode width is increased, it will reduce the surface area of the electrolyte and also the amount of active species produced also decreasing.

For the gap between the electrodes to design multiple planes, the same value is used as in the design of the plane that is between 50 and 250 μm. In response to the voltage, resulting flows

are plotted in **Figure 20**. Based on these figures, we can see that the greater the gap between the electrodes, the higher the current response. On the sidelines of the electrode 250 μm, the reaction flow reaches a maximum value of 26.4 A/m,which is doubled in value compared the design of the plane. This is because the number of cells for multiple planar design is twice that of the coplanar design that has 40 pairs of cells, so, with the increase in the number of cells, allowing for a number of active species of a higher existence on the active surface **Table 1** shows the comparison of parameters between planar and interdigital electrode supercapacitor design.

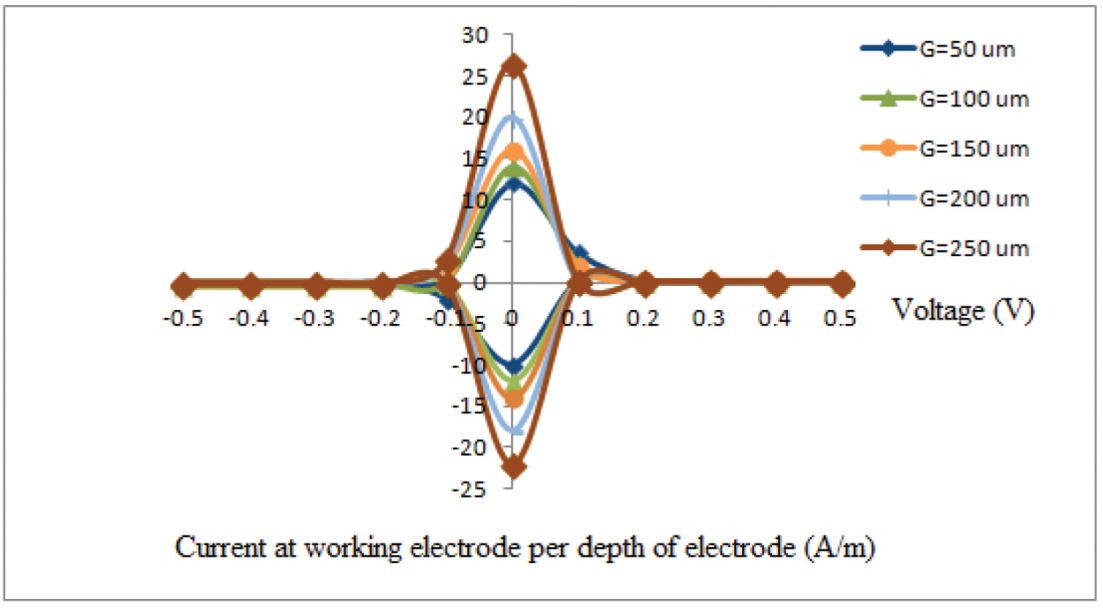

Figure 20. Cyclic voltammetry for various values of the width interdigital electrode.

Parameter	Planar	Double stacked
Number of fingers	20	Total 40 (20 top, 20 bottom)
Layout size (mm^2)	8.8	8.8
Thickness of cell (μm)	925	1950
Maximum charge (voltage input 3 V) (pC)	6.77	15.50
Specific capacitance (mF/cm^{-2})	0.22	0.48
Specific power (mW/cm^{-2})	0.99	2.18

Table 1. Comparison of parameters between planar and interdigital electrode supercapacitor design.

6. Conclusions

Energy harvesting system has a high potential as an alternative power especially in biomedical implant devices such as pacemakers. Due to the disadvantages such as short lifetime and

containing a finite amount of depletable chemical energy of lithium-ion batteries, the patients using heart pacemaker have to replace the battery once every 5–10 years. To avoid any powering unit replacement, a renewable energy generation and storage system could become a vital solution. From this research, it can be concluded that double-stacked MEMS interdigital supercapacitor has same layout, only slightly thicker compared with the planar structure due to double stacking, but with much superior charging capacity. For both planar and double-stacked MEMS interdigital supercapacitor designs, the electrodes width, length, and gap between electrode fingers were fixed at 50, 500, and 50 μm, respectively. Furthermore, the planar and double-stacked MEMS interdigital supercapacitor designs were simulated using COMSOL ver.4.2a for electrical performance verification such as cyclic voltammetry and charge discharge performance. For cyclic voltammetry performance, applied voltage range is set to −0.5 to 0.5 V. For capacitance performance, it is observed that capacitance increases linearly with increasing number of cell, length of fingers, and width of fingers due to charge interactions among adjacent cells. The simulation results show that the planar structure has a charging capacity of 6.77 pC and the double-stacked structure has a charging capacity of 15.5 pC. Furthermore, for specific capacitance, it is observed that for planar structure is 0.22 mF/cm^{-2} and for double-stacked structure is 0.48 mF/cm^{-2}, while for specific power, the planar structure is 0.99 mW/cm^{-2} and for double-stacked structure is 2.18 mW/cm^{-2}. For charge discharge curve, it is observed that the curves are almost linear in the potential range. These results highlight the superiority of the double-stacked MEMS interdigital supercapacitor design compared with its planar counterpart in terms of charging capacity and electrical performance, thus making it favorable for powering heart pacemakers.

Author details

Hafzaliza Erny Zainal Abidin, Azrul Azlan Hamzah*, Jumril Yunas,
Mohd Ambri Mohamed and Burhanuddin Yeop Majlis

*Address all correspondence to: azlanhamzah@ukm.edu.my

Institute of Microengineering and Nanoelectronics (IMEN), The National University of Malaysia, Bangi, Selangor, Malaysia

References

[1] Joo Hwan Sung, Se Joon Kim and Kun Hong. Fabrication of all solid state electrochemical microcapacitors. Journal of Power Sources. 2004;133(2):312–319.

[2] Venkateswara Sarma Mallela, V Ilankumaran and N Srinivasa Rao. Trends of cardiac pacemaker. Indian Pacing & Electrophysiology Journal. 4(4):201–212.

[3] Pei Hong Wang, Xu Hu Dai, Dong Ming Fang and Xiao Lin Zhao. Design, fabrication and performances of a new vibration based electromagnetic micro power generator. Microelectronics Journal. 2007;38(12):1175–1180.

[4] Craig L Schmidt and Paul M Skarstad. The future of lithium and lithium ion batteries in implantable medical devices. Journal of Power Sources. 2001;97–98:742–746.

[5] Hafzaliza Erny Zainal Abidin, Azrul Azlan Hamzah, Burhanuddin Yeop Majlis, Jumril Yunas, Norihan Abdul Hamid, Ummikalsom Abidin. Electrical characteristics of double stacked Ppy-PVA supercapacitor for powering biomedical MEMS devices. Microelectronic Engineering Dai. 2013;111:374–378.

[6] Noraini Marsi, Burhanuddin Yeop Majlis, Azrul Azlan Hamzah and Faisal Mohd Yasin Development of high temperature resistance of 500°C employing silicon carbide (3C-SiC) based MEMS pressure sensor. Microsystems Technologies. 2015;21:319–330.

[7] Jumril Yunas, Juliana Johari, Azrul Azlan Hamzah, Mimiwaty, Ille C Gebeshuber and Burhanuddin Yeop Majlis. Design and fabrication of MEMS micropumps using double sided etching. Journal of Microelectronics and Electronic Packaging. 2010;7:44–47.

[8] Azrul Azlan Hamzah, H E Zainal Abidin, B Yeop Majlis, M Mohd Nor, A Ismardi, G Sugandi, et al. Electrochemically deposited etched membranes with precisely sized micropores for biological fluids microfiltration. Journal Micromechanics and Microengineering. 2013;23:1–9.

[9] A Leela Mohana Reddy, F Estaline Amitha, Imran Jafri and S Ramaprabhu. Asymmetric flexible supercapacitor stack. Nanoscale Research Letters. 2008; 3(145):145–151.

[10] Hafzaliza Erny Zainal Abidin, Azrul Azlan Hamzah and Burhanuddin Yeop Majlis. Design of interdigital structured supercapacitor for powering biomedical devices. In: Regional Symposium on Micro and Nanoelectronics; Kota Kinabalu, Sabah, Malaysia. IEEE; 2011.

[11] Wei Sun, Ruilin Zheng and Xuyuan Chen. Symmetric redox supercapacitor based on micro fabrication with three dimensional polypyrrole electrodes. Journal of Power Sources. 2010;195(20):7120–7125.

[12] M Jayalakshmi and K Balasubramanian. Simple capacitors to supercapacitors – An overview. International Journal of Electrochemical Science. 2008;3:1196–1217.

[13] Maximilian Kaus, Julia Kowal and Dirk Uwe Sauer. Modelling the effects of charge redistribution during self discharge of supercapacitors. Electrochimica Acta. 2010;55(25):7516–7523.

[14] Caiwei Shen, Xiaohong Wang, Wenfeng Zhang and Feiyu Kang. A high performance three dimensional micro supercapacitor based on self supporting composite materials, Journal of Power Sources.2011:196(23):10465-10471.

[15] M Paeschke, U Wollenberger, C Kohler, T Lisec, U Schnakenberg and R Hintsche. Properties of interdigital electrode arrays with different geometries. Analytica Chimica Acta. 1995;2670(136):126–136.

[16] Meng Deng, Xi Yang, Musa Silke, Weiming Qiu, MingSheng Xu, Gustaaf Borghs et al. Electrochemical deposition of polypyrrole/graphene oxide composition on microelectrodes towards tuning the electrochemical properties of neural probes. Sensors and Actuators B. 2011;158(1):176–184.

[17] Marin S. Halper and James C Ellenbogen. Supercapacitor: A brief overviews. 2006:1–41.

[18] Hyuck Lee, Hyeongkeun Kim, Mi Suk Cho,Jaeboong Choi and Youngkwan Lee. Fabrication of polypyrrole (Ppy)/carbon nano tube (CNT) composite electrode on ceramic fabric for supercapacitor applications. Electrochimica Acta. 2011;56(22):7460–7466.

[19] R Ramya, R Sivasubramanian and M V Sangaranarayanan. Conducting polymers based electrochemical supercapacitor-progress and prospects. Electrochimica Acta. 2013;101:101–129.

[20] Farah Alvi, Manoj K Ram, Punya A Basnayaka, Elias Stefanakes, Yogi Goswami and Ashok Kumar. Graphene polyethylenedioxythiophene conducting polymer nanocomposite based supercapacitor. Electrochimica Acta. 2011;56(25):9406–9412.

[21] Mustafa Gullu and Deniz Yigit. A novel asymmetric pseudocapacitor based on poly (5,12-dihydrothieno[3,4:2,3] [1, 4] dioxocino[6,7-b] auinoxaline) coated graphite anode and poly(ethylenedioxythiophene)coated graphite cathodes. Electrochimica Acta. 2012;162(15–16):1434–1442.

[22] Graeme A Snook, Pon Kao and Adam S Best. Conducting polymer based supercapacitor devices and electrodes. Journal of Power Sources. 2011;196(1):1–12.

[23] Wei Sun and Xuyuan Chen. Fabrication and tests of a novel three dimensional micro-supercapacitor. Microelectronic Engineering. 2009;86(4–6):1307–1310.

[24] Y Q Jiang, Q Zhou and L Lin. Planar MEMS supercapacitor using CNT forests. In: 2009 IEEE 22nd International Conference on Micro Electromechanical Systems; IEEE; Sorrento, Italy. 2009. pp. 587–590.

[25] Majid Beidaghi and Chunlei Wang. Micro supercapacitor based on three dimensional interdigital polypyrrole/C-MEMS electrodes. Electrochimica Acta. 2011;56(25):9508–9514.

[26] Available from: http://www.embedded.com/print/4403423. 10 energy Harvesting solutions for 2012.

[27] Azrul Azlan Hamzah, Burhanuddin Yeop Majlis and Ibrahim Ahmad. Deflection analysis of epitaxially deposited polysilicon encapsulation for MEMS devices. In: IEEE,

editor. IEEE International Conference Semiconductor Electronics; Kuala Lumpur, Malaysia. 7–9 September 2004; 2004.

[28] Norazreen Abdul Aziz, B Bais, A A Hamzah and B Y Majlis. Characterization of HNA etchant for silicon microneedles array fabrication. In: IEEE 8th International Conference on Semiconductor Electronics; IEEE; Johor Bharu, Malaysia, 2008. pp. 203–206.

[29] N A Aziz, B Bais, A A Hamzah and B Y Majlis Optimization of HNA etching parameters to produce high aspect ratio solid silicon microneedles. Journal of Micromechanics and Microengineering. 2012;22(9)1-10.

[30] Hainan Wang and Laurent Pilon. Physical interpretation of cyclic voltammetry for measuring electric double layer capacitances. Electrochimica Acta. 2012; 64:130–139.

[31] Available from: https://www.comsol.com/community/exchange/203/. Robert Palumbo, Valparaiso University, Email: Robert.Palumbo@valpo.edu

[32] Alessandro Lavacchi, U Bardi, S Caporali, A Fossati and I Perissi. Cyclic voltammetry simulation at microelectrode arrays. In: Proceedings of Comsol Users Conference 2006; Bangalore, India. 2006.

IntechOpen